Edinburgh Research Explorer

Experimental Characterisation of the Fire Behaviour of Thermal Insulation Materials for a Performance-Based Design Methodology

Experimental Characterisation of the Fire Behaviour of Thermal Insulation Materials for a Performance-Based Design Methodology

Abstract

A novel performance-based methodology for the quantitative fire safe design of building assemblies including insulation materials has recently been proposed. This approach is based on the definition of suitable thermal barriers in order to control the fire hazards imposed by the insulation. Under this framework, the concept of "critical temperature" has been used to define an initiating failure criterion for the insulation, so as to ensure there will be no significant contribution to the fire nor generation of hazardous gas effluents. This paper proposes a methodology to evaluate this "critical temperature" using as examples some of the most common insulation materials used for buildings in the EU market, i.e. rigid polyisocyanurate foam (PIR), rigid phenolic foam (PF), rigid expanded polystyrene foam (EPS) and low density flexible stone wool (SW). A characterisation of these materials, based on a series of ad-hoc Cone Calorimeter and thermo-gravimetric experiments, serves to establish the rationale behind the quantification of the critical temperature. The temperature of the main peak of pyrolysis, obtained from differential thermo-gravimetric analysis (DTG) under a nitrogen atmosphere at low heating rates, is proposed as the "critical temperature" for materials that do not significantly shrink and melt, i.e. charring insulation materials. For materials with shrinking and melting behaviour it is suggested that the melting point could be used as "critical temperature". Conservative values of "critical temperature" proposed are 300 °C for polyisocyanurate, 425 °C for phenolic foam and 240 °C for expanded polystyrene. The concept of a "critical temperature" for the low density stone wool is examined in the same manner and found to be non-applicable due to the inability to promote a flammable mixture. Additionally, thermal inertia values required for the performance-based methodology are obtained for PIR and PF using a novel approach, providing thermal inertia values within the range $4.5 - 6.5 \cdot 10^3$ $W^2 \cdot s \cdot K^{-2} \cdot m^{-4}$.

Keywords

Insulation materials; Fire hazard; Pyrolysis onset; Performance-based design; Critical temperature; Fire performance; Flammability

Nomenclature

c_p	specific heat capacity ($J \cdot kg^{-1} \cdot K^{-1}$)
$erfc$	error function
h	heat transfer coefficient ($W \cdot m^{-2} \cdot K^{-1}$)
k	conductivity ($W \cdot m^{-1} \cdot K^{-1}$)
L	thickness or length (m)
$\dot{m}$	mass flow ($kg \cdot s^{-1}$)

$\overline{Nu}_L$	Nusselt number (-)
Ra_L	Rayleigh number (-)
t	time (s)
$\dot{q}''$	heat flux (W·m^{-2})
T	temperature (K or °C)
x	space (m)

Greek letters

α	absorptivity (-)
ρ	density (kg·m^{-3})
κ	thermal diffusivity (m^2·s^{-1})
σ	Stefan–Boltzmann constant (W·m^{-2}·K^{-4})

Subscripts

c	characteristic
$conv$	of convection
cr	Critical
e	external/incident radiation
ig	of ignition
P	of pyrolysis
r	of radiation
s	of the surface
T	total, considering convection and radiation
∞	of ambient

Acronyms

CHF	critical heat flux
CO	carbon monoxide
CO_2	carbon dioxide
DTG	differential thermo-gravimetric analysis
EPS	expanded polystyrene
LOESS	locally weighted scatterplot smoothing
O_2	Oxygen
PIR	rigid polyisocyanurate foam
PF	rigid phenolic foam
SW	stone mineral wool
TGA	thermo-gravimetric analysis

1. Introduction

At present, the fire safe use of insulation materials in buildings design is established on the basis of material classification and pass-fail criteria obtained from standard testing. This is represented in the European Union as the *reaction-to-fire* [1] and *fire-resistance frameworks* [2], respectively. The *reaction-to-fire* framework consists of a material classification, known as *Euroclasses*, based on the

non-combustibility test [3], *the heat of combustion test* [4], an *ignitability test* [5] and the *single burning item test* (SBI) [6]. Prescriptive design standards require the use of certain classes for specific uses. The *fire-resistance* framework is based on the standard furnace test [2], in which the thermal insulation (I) and integrity (E) criteria are evaluated for non-loadbearing elements. The International Building Code [7] and NFPA 5000 [8] provide similar prescriptive frameworks as the EU framework, but also requiring a flammability classification for insulation materials based on a flame spread test such as ASTM E84 [9], and mandatorily considering a thermal barrier, the performance of which is evaluated by a series of pass-fail criteria based on the ASTM E119 test [10] and/or the *room-corner test* [11]. *Hidalgo et al.* (2015a) previously discussed the limitations of these testing methods when attempting to provide a quantifiable level of fire safety for construction systems that incorporate insulation materials [12]. A quantitative performance assessment method was proposed based on a mapping of the different levels of hazard represented by the use of insulation materials in buildings [12], together with a series of control measures so as to mitigate them. This methodology intends to provide a generalised quantitative approach to mitigate the fire risks from insulation materials in buildings, which is complementary to the existing prescriptive methods. As noted by *Hidalgo et al.*, the onset of hazard from a combustible material can be conservatively established as the 'onset of pyrolysis'. This concept is not new, and was used by *Drysdale* [13], who theoretically demonstrated the propensity of insulation materials to rapidly reach the onset of pyrolysis due to their very low thermal inertia. *Drysdale* concludes that "*these features, rather than the propensity to produce smoke and toxic gases should be regarded as the principal hazard, and measures for their control urgently sought*".

The proposed methodology relies on the well-known approach of incorporating thermal barriers in order to control the onset of pyrolysis from the insulation. In quantifying the effectiveness of the thermal barriers, it is necessary to establish a series of inputs such as (1) a critical temperature that describes the onset of pyrolysis, (2) the thermal properties of the barrier and insulation material, and (3) the boundary condition (fire inputs) to be considered. The former implies the necessity of characterising the failure criterion and material behaviour associated to the specific insulation, while the latter implies the need of further characterising the heating conditions from real fires so that appropriate fire scenarios can be considered for design strategies. Initial steps have already been taken towards the use of this approach for the generation of tools to design adequately thermal barriers [14], and based on the formulation already presented by *Hidalgo et al.* [12]. These tools, in relatively early stages of conception, present a potential solution for the selection of suitable barriers for specific fire scenarios so as to optimise designs considering fire safety as a quantitative parameter.

1.1. The concept "critical temperature" as failure criterion

The 'onset of pyrolysis' can be used to establish the initiation of hazard on the basis that it is intrinsically related to the degradation of a material. This could result in the generation of combustible gases but it could also result in loss of functionality. Material properties change through pyrolysis and

these changes could have an effect on mechanical and thermal behaviour (e.g. charring, loss of mechanical strength, loss of bonding, decrease in thermal conductivity, etc.). Different approaches may be followed in order to provide quantifiable parameters that represent these changes and to establish if the changes lead to a hazard. The quantification of the hazard needs to incorporate a complex combination of mechanical deterioration properties and the generation of combustible gases. Quantifying mechanical deterioration requires the description of loads, restraint, and thermal expansion. Quantifying the generation of combustible gases requires the assessment of pyrolysis rates. Many different approaches have been followed to quantify pyrolysis and this subject is still a matter of research, in particular when it comes to developing simplified approaches that can be used as engineering tools. The authors recognise that there are numerous pyrolysis models [15, 16], but these are generally applied at a research level rather than as engineering tools, essentially due to the high level of uncertainty in defining multiple input parameters and the high required user expertise utilising these packages. Indeed, design tools for the characterisation of this hazard ideally require both simplicity and reliability in predicting the physical mechanisms so as to be applied by practitioners.

The approach proposed by *Hidalgo et al.* [12, 14] is based on the definition of a critical temperature for the surface of the specific insulation material as a failure criterion. The critical temperature should be interpreted here as a means to quantify the onset of a process. If the process is a continuous function of the temperature, such as pyrolysis, the critical temperature only represents a threshold beyond which the process is deemed significant. This approach has been used very frequently when addressing fire problems because in fires flow fields, chemistry and materials are extremely complex and do not allow establishing more fundamental parameters. *Drysdale* [17] reviews many of these critical parameters (e.g. ignition temperature, critical mass flux for extinction, critical mass transfer number, etc.). The definition of a critical parameter can be used to deliver a more or less conservative criterion. The choice of a critical pyrolysis temperature, as defined through differential thermo-gravimetric analysis (DTG) under a nitrogen atmosphere at low heating rates and Cone Calorimeter [18] tests is argued as a conservative critical temperature [12]. If this temperature is then defined as a target, the design is simplified to a selection of suitable thermal barriers that, as a function of their thermal properties, can prevent the attainment of this critical temperature. The analysis can be performed for any fire scenario that the designer or stakeholders deem appropriate. This approach has the potential to deliver a simplified methodology that is capable of yielding a quantitative assessment of performance.

1.2. Research objective

The aim of this manuscript is to provide an analysis on the definition of the critical temperature for some of the most common insulation materials in the EU market, based on the characterisation of the flammability and the solid-phase thermal degradation of these materials. In order to achieve this, a series of ad-hoc experiments is presented using the Cone Calorimeter [18] and thermo-gravimetric techniques.

Complementary to the assessment of the critical temperature, a characterisation of the thermal properties of these materials prior to the pyrolysis onset is presented.

Therefore, the work presented hereby complements the work presented by *Hidalgo et al.* [12], which mainly consisted of a careful review of the limitations of current prescriptive frameworks applicable in the EU and the US for the fire safe design of insulated assemblies, a suggested redefinition of the failure criteria for insulation materials and the formulation of a performance-based design methodology.

2. Experimental programme description

2.1. Materials

The studied insulation materials comprised low density flexible stone wool (SW), rigid phenolic foam (PF), expanded polystyrene (EPS) and three types of rigid polyiscocyanurate foam (PIR). Stone wool is a fibrous inorganic material spun from mainly volcanic basalt and diabase rocks and organic binders. Expanded polystyrene, rigid phenolic foam, and rigid polyisocyanurate foam are classified as plastics, i.e. organic polymers that have only partially reversible deformability [19]. Among this category, EPS belongs to the group of thermoplastics, while PF and PIR correspond to thermosets. These plastics are manufactured as rigid closed-cell polymers by blowing a gas through the entire structure of the foam. At present, the blowing agents mainly utilised are n-Pentane, iso-Pentane, cyclo-Pentane and hydrofluorocarbons that have zero ozone depleting potential [20].

Three different PIR foams from different suppliers were selected in order to assess their differences in performance and establish a conservative value of the critical temperature. Polyisocyanurate, which is manufactured based on the mix of an organic isocyanate component and an isocyanate-reactive component, is known to present several possible formulations depending on the isocyanate-reactive component used, which determines its thermal stability [21]. Despite the fact that several manufacturers provide this product under the same denomination (PIR), there is large uncertainty in the formulation used, as well as in distinguishing it from polyurethane rigid foams (PUR). As a matter of fact, one of the foams was originally acquired in the belief that it corresponded to PUR, however this was found to actually be a different formulation of PIR.

Standard thermo-physical properties at ambient temperature for the specific insulation materials being studied are presented in

Table 1. Values of thermal conductivity and specific heat capacity are obtained from common manufacturer datasheets.

Table 1. Common thermo-physical properties from insulation materials at ambient temperature

Material	Main characteristics	Thermal conductivity /W ·m^{-1}·K^{-1}	Density (measured) /kg·m^{-3}	Specific heat capacity /J ·kg^{-1}·K^{-1}	Thermal inertia (calculated) /W^2·s·K^{-2}·m^{-4}
SW	Flexible fibrous wool	0.034-0.044	40	840	1142-1478
PIR	Rigid closed cell – supplied as foil faced boards	0.022-0.028	32	1500	1066-1344
PF	Rigid closed cell – supplied as foil faced boards	0.021-0.024	38	1500	1197-1368
EPS	Rigid closed cell – supplied as uncovered boards	0.031-0.038	10	1500	465-570

It should be noted that the purpose of choosing different types of materials is not to seek a classification nor a comparison, but to demonstrate the applicability of the methodology to determine the critical temperature for materials of different nature. The materials chosen are all commonly used insulation materials that experience charring, melting, or that consist of inorganic compounds and organic binders.

### 2.2. Cone Calorimeter ad-hoc experiments

A Cone Calorimeter apparatus [18] was used to determine flammability properties for the studied insulation materials. This apparatus provides a standardised heat exposure for testing solid samples under the presence of a pilot spark, and allows for the measurement of the time-to-ignition, mass loss, and oxygen, carbon dioxide and carbon monoxide emissions.

Samples were prepared with dimensions of a nominal surface area of 90 mm x 90 mm and a non-standard thickness of 100 mm. While the ideal dimensions for bench-scale testing using the Cone Calorimeter, or similar type of instrument, have been determined to be 100 mm x 100 mm [22], slightly narrower samples were prepared for consistency, since additional tests using the FPA [23] were performed in a parallel project focused on the smouldering behaviour of rigid closed-cell PIR foam [24]. A thickness of 50 mm is the limit thickness under standard operation. Nevertheless, for this study 100 mm was selected to achieve a time-to-ignition that was not affected by the back end boundary condition. This was confirmed by verifying that the thermal wave did not reach the bottom of the sample earlier than the ignition time. This can be estimated by Eq. (1), which is easily satisfied by 100 mm insulation samples due to the very low thermal diffusivity:

$$L > 4 \cdot \sqrt{\kappa \cdot t_{ig}} \tag{1}$$

where L is the thickness of the sample, κ is the thermal diffusivity and t_{ig} is the ignition time.

Closed-cell rigid foams such as PIR and PF are often provided by manufacturers as boards with a protective layer (foiled facing) on the surface, especially in the European market. The protective layer with relatively low emissivity was expected to have an impact on the results from the tests. However, since the present work aims to provide material properties of the insulation rather than those of the composite, the protective layer was removed by peeling it off from the surface, thus leaving the foam core exposed. It is clear that if the objective of the work was to study the material as used, then it will be appropriate to test the layer independently as well as the composite. Material samples without the protective layer, as prepared for testing, are shown in Figure 1.
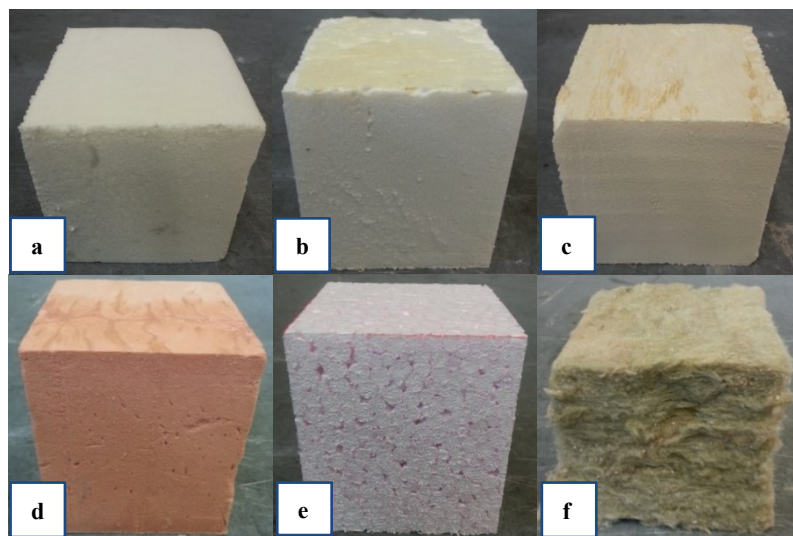
Figure 1. Samples of insulation materials prior to testing.
(a) PIRa (b) PIRb (c) PIRc (d) PF (e) EPS (f) SW

Samples were individually wrapped in aluminium foil, leaving only the top surface exposed, and then wrapped by two 3 mm thick layers of ceramic paper at the sides and bottom as shown in Figure 2. The two layers of ceramic paper were used in order to reduce the thermal gradient on the surface of the sample sides. It should be noted that an ideal adiabatic boundary condition at the sides will always be unattainable with this set-up since the conductivity of the ceramic paper is higher than the materials tested[1]. The samples were tested using a horizontal orientation.

---
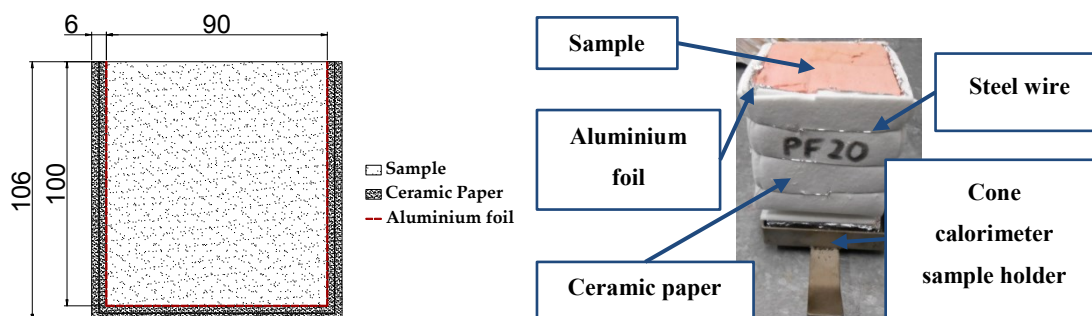
[1] Thermal conductivity of ceramic paper: 0.08 and 0.11 $W \cdot m^{-1} \cdot K^{-1}$ at 600 and 800°C, respectively.

Figure 2. Sample preparation for Cone Calorimeter experiments (dimension units in millimetres)

Samples were systematically tested decreasing the incident radiant heat flux (also referred to as external heat flux) to determine the lowest heat flux at which piloted ignition occurred, hereby denoted as critical heat flux (CHF). The CHF was obtained by iterating between heat fluxes where it ignited and those where it did not. The standard definition of ignition before 10 minutes was used to determine if piloted ignition occurred. A summary of the different test configurations and measured parameters for this experimental programme are presented in Table 2 below.

Table 2. Summary of test conditions with the Cone Calorimeter

Material	Configuration	Incident radiant heat flux range /kW·m^{-2}	Measured parameters
PIRa	**Nominal sample size:** 90 mm x 90 mm x 100 mm **Exposed surface:** Without protective layer **Wrapping:** 2 layers of ceramic paper + 1 layer of foil **Back boundary condition:** Ceramic board (25 mm) **Orientation:** Horizontal	From CHF to 65 (2 repetitions)	- Time-to-ignition - O$_2$, CO$_2$ and CO gas species - Mass loss
PIRb			
PIRc			
PF			
EPS	**Nominal sample size:** (a) 90 mm x 90 mm x 100 mm (b) 90 mm x 90 mm x 50 mm **Exposed surface:** No protective layer **Wrapping:** 2 layers of ceramic paper + 1 layer of foil **Back boundary condition:** Ceramic board (25 mm) **Orientation:** Horizontal		
SW	**Nominal sample size:** 90 mm x 90 mm x 100 mm **Rest of the configuration as EPS**	Up to 88	

2.3. Thermo-gravimetric experiments

A METTLER-TOLEDO TGA/DSC 1® apparatus was used in order to assess the thermal degradation at material scale. The TGA apparatus consists of a furnace with a horizontal arm with a load cell for the sample and reference crucible, which is used to control the heating rate. A gas controller was installed in the apparatus, so that the concentration of oxygen in the atmosphere inside the furnace chamber could be controlled. The crucibles, or sample holders, used for this experimental programme were made of alumina (aluminium oxide) and were of 70 µL capacity.

Each material was tested under two different atmospheric conditions, i.e. air and nitrogen at 50 ml·min^{-1}, and under four different heating rates: 2.5, 5, 10 and 20 °C·min^{-1}. Dual replicates were used to check the repeatability of the results. The nominal sample size was 2 mm x 2 mm x 2 mm for plastic foams and 3 mm diameter by 2 mm thickness for stone wool. Since these materials are characterised by their very low density (< 40 kg·m^{-3}), this sample size corresponded to a mass lower than 1 mg for plastic

foams and a mass lower than 25 mg for stone wool. Small sample sizes and low masses are required to achieve good results since a kinetic regime is pursued. Thus, it was anticipated that no significant mass or heat transfer effects would be present. The samples from plastic foams were prepared by cutting small pieces of the original material, since the material is relatively homogeneous. On the contrary, since stone wool is a heterogeneous material, the stone wool samples were prepared by mixing a sample of fibres extracted from the original wool and fitting them into the crucible. This test condition justifies the higher sample mass in comparison to the foams. A more homogeneous sample was expected by proceeding with this technique. A list of the total number of experiments is presented in Table 3. As general practice, experiments ran from 25 °C up to 800 °C.

Table 3. List of general TGA experiments

Material	Sample configuration	Heating rate /°C·min^{-1}	Atmospheric condition	Temperature range
SW	Nominal sample size: Ø3 mm x 2 mm Nominal initial mass: < 25 mg	20, 10, 5, 2.5 (2 repetitions)	(a) 50 ml·min^{-1} of N$_2$ (b) 50 ml·min^{-1} of air	25 – 800 °C
PIRa	Nominal sample size: Cut 2 mm x 2 mm x 2 mm Nominal initial mass: < 1 mg			
PIRb				
PIRc				
PF				
EPS				

3. Analysis methodology

3.1. Parameters for the critical temperature assessment

The first steps towards establishing the criterion for selecting the critical temperature require the evaluation of thermal properties of the studied insulation materials. The selected methodology for assessing thermal properties is based on the transient heat transfer analysis a semi-infinite inert solid, so as to determine an ignition temperature at the surface. This enables to establish the evolution of the surface temperature, until the attainment of a critical temperature. In piloted ignition studies, an ignition temperature, T_{ig}, corresponds to the critical temperature, while here the critical temperature is the pyrolysis temperature, T_P. This method is used for consistency with the critical temperature approach, rather than one based on a critical mass flux [25], i.e. both are delimited to engineering terms of surface temperature. This methodology has been extensively studied by many authors, a summary of which can be found elsewhere [26]. The particular formulation considered for this work is the one presented by *Long et al.* [27]. The time to achieve the pyrolysis temperature at the surface of the solid material can be obtained according to Eq. (2):

$$\frac{(T_P - T_\infty)}{T_c} = \left[1 - exp\left(\frac{t_P}{t_c}\right) \cdot erfc\left(\left(\frac{t_P}{t_c}\right)^{1/2}\right)\right] \qquad (2)$$

where T_P and t_{iP} are the temperature and time of pyrolysis onset, T_∞ is the ambient temperature, $erfc$ is the complementary Gaussian error function, T_c is the characteristic surface temperature defined as Eq. (3) and t_c is the characteristic time defined as Eq. (4):

$$T_c = \frac{\alpha \cdot \dot{q}_e''}{h_T} \tag{3}$$

$$t_c = \frac{k\rho c}{(h_T)^2} \tag{4}$$

where α is the absorptivity of the exposed surface, $\dot{q}_e''$ is the external heat flux, h_T is the global heat transfer coefficient of losses and $k\rho c$ is the thermal inertia. The global heat transfer coefficient of losses, at the time that the surface achieves the pyrolysis temperature, can be defined as:

$$h_T = h_{conv} + h_r = h_{conv} + \varepsilon \cdot \sigma \cdot \frac{(T_P^4 - T_\infty^4)}{(T_P - T_\infty)} = h_{conv} + \varepsilon \cdot \sigma \cdot (T_P^2 + T_\infty^2) \cdot (T_P + T_\infty) \tag{5}$$

where h_c is the convective heat transfer coefficient, ε is the emissivity of the surface, σ is the Stefan–Boltzmann constant and T_∞ is the ambient temperature. The definition of the convective heat transfer coefficient is based on the estimation of the Nusselt number for the free convection of a horizontal hot plate [28], as noted in Eq. (6):

$$\overline{Nu}_L = 0.54 \cdot Ra_L^{1/4} = \frac{h_{conv} \cdot L_c}{k_{air}} \tag{6}$$

where Ra_L is the Rayleigh number k_{air} is the conductivity of the air and L_c is the characteristic length.

The pyrolysis temperature can often be measured if a thermocouple is positioned close to the surface. This is however a complicated task which may not be applied for any material, as for the case of the studied materials due to several reasons such as (1) brittle nature of the foams, (2) large thermal gradient expected at the surface due to low conductivity, and (3) expected heat losses through the thermocouple inserted in an insulated medium.

If temperature measurements are not feasible, the pyrolysis temperature can be calculated assuming that the steady-state is achieved for the heat balance at the surface. For this case, the net heat flux through the surface of the material can be assumed to be null, i.e.:

$$\dot{q}_{net}'' = -k \cdot \left. \frac{\delta T}{\delta x} \right|_{x=0} \approx 0 \tag{7}$$

where k is the conductivity of the material and $\left. \frac{\delta T}{\delta x} \right|_{x=0}$ is the thermal gradient at the surface. Though *Mowrer* [29] indicates the potential inaccuracy of this approach, due to non-negligible values of the net heat flux through the solid surface during the steady-state, numerical analyses demonstrate that the conducted flux is lower than 7 % of the absorbed radiant heat flux for the specific case of materials with very low thermal conductivity [30]. Thus, the heat balance at the surface can be expressed as:

$$\alpha \cdot \dot{q}''_{cr} - h_c \cdot (T_P - T_\infty) - \varepsilon \cdot \sigma \cdot (T_P^4 - T_\infty^4) = \dot{q}''_{net} \approx 0 \qquad (8)$$

Under many conditions it has been demonstrated that the time difference between the onset of pyrolysis and piloted ignition is very small, therefore $t_p \approx t_{ig}$ and $T_p \approx T_{ig}$ and the critical external heat flux for piloted ignition $\dot{q}''_{cr}$ obtained experimentally can be used to determine the pyrolysis temperature [27]. Therefore, the expression to calculate the pyrolysis temperature can be written as follows:

$$T_P = T_\infty + \frac{\alpha \cdot \dot{q}''_{cr}}{h_T} \qquad (9)$$

It should be noted that since the total heat transfer coefficient depends on the surface temperature, the pyrolysis temperature and the total heat transfer of losses are calculated by solving iteratively the system of non-linear equations consisting of Eq. (5) and (9).

While the quantification of the ignition temperature provides an assessment of the flash point under the specific mixing conditions of the Cone Calorimeter, the critical temperature at the surface of the insulation, pyrolysis temperature, is potentially achieved prior to the ignition temperature. Information with regard to the thermal degradation mechanisms of the material is thus essential for the validation of the former assumption and, therefore for the interpretation of the critical temperature selection.

Thermo-gravimetric techniques are usually applied to characterise the processes of thermal degradation of the solid-phase (pyrolysis and oxidation reactions), based on the determination of mass loss with respect to temperature increases [31]. The differential form of a TGA curve (DTG) is commonly used to quantify the rates of mass loss from each of the different reactions, which can be characterised by a series of kinetic parameters representative of an Arrhenius' type expression. Attempts can be made to determine the kinetic parameters of each reaction to be implemented in complex pyrolysis models [15], however this is a task often tackled by using optimisation techniques, which invokes a lot of uncertainty as multiple kinetic parameters can provide good fitting without representing the actual activation energy from the chemical reaction [32]. This process may even be more complicated if multiple reactions overlap, as is typical, thus deconvolution techniques being necessary to isolate each of the reactions [33].

Nonetheless, the identification of the main thermal degradation reactions can be assessed by interpreting the peaks of mass loss rate, i.e. peaks in the DTG curve. This information is vital to assess the onset of pyrolysis, in which extrapolation to a specific value of critical temperature must be done carefully due to the dependency of the rate of mass loss to the heating rate.

3.2. Thermal inertia characterisation

Long et al. applied a first-order Taylor series expansion to Eq. (2) in order to determine simplified correlations between the time-to-ignition and the external heat flux, based on two domains defined by the relation between the pyrolysis time and the characteristic time (t_p/t_c):

$$t_P^{-\frac{1}{2}} = \frac{2}{\sqrt{\pi}} \cdot \frac{\alpha}{\sqrt{k\rho c}} \cdot \frac{\dot{q}_e''}{(T_P - T_\infty)} \qquad \text{with } t_p/t_c \to 0 \qquad (10)$$

$$t_P^{-\frac{1}{2}} = \frac{\sqrt{\pi} \cdot h_T}{\sqrt{k\rho c}} \cdot \left[1 - \frac{(T_P - T_\infty)}{T_c} \right] \qquad \text{with } t_p/t_c \to \infty \qquad (11)$$

These expressions provide a simplified way to determine the thermal inertia of materials based on experimental values of time-to-ignition (t_P) for different levels of external heat flux ($\dot{q}_e''$). The approach consists in finding a value of thermal inertia that provides good fitting of Eq. (10) or (11) with respect to the experimental data. However, due to the relatively low thermal inertia, the time to achieve the onset of pyrolysis is very short, therefore for insulation materials it is anticipated that these expressions would provide an inaccurate estimation of $k\rho c$ in practice. Consequently, the authors suggest to compare the experimental results (time-to-ignition and external heat flux) directly to the non-dimensional solution for the surface temperature of the semi-infinite plate shown in Eq. (2), and from which Eq. (10) or (11) originally are derived. The experimental data are thus non-dimensionalised as the function $f(t_p)$ defined at the left-hand side terms of Eq. (12). Values of thermal inertia are sought in order to satisfy a good fitting between the non-dimensional solution for the surface temperature of the semi-infinite plate, given by the right-hand side term of Eq. (12), and the experimental external heat flux plotted as the function $f(t_p)$ versus its respective time-to-ignition:

$$f(t_p) = \left[1 - \frac{(T_P - T_\infty)}{T_c} \right] = exp\left(\frac{t_P}{t_c}\right) \cdot erfc\left(\left(\frac{t_P}{t_c}\right)^{1/2}\right) \qquad (12)$$

The main advantage from this methodology is that it allows to verify whether the underpinning hypothesis from this analysis is met, i.e. to verify the semi-infinite solid behaviour from the samples until the ignition is achieved. The use of data points that do not meet this assumption would lead to incorrect quantification of thermal inertia [29].

4. Results

The main visual observations from experiments indicate that PIR and PF are charring materials that achieve a very fast ignition for heat fluxes above the critical, followed by a decay of the flame until it quenches or with flaming just obtained at the edges. The char residue at the surface experiences significant oxidation (smouldering), the rate of which is dependent on the external heat flux. Expanded polystyrene, however, shrinks quickly after heat exposure, following melting and eventual volatilisation and ignition, while stone wool did not proceed to ignition. A series of results that further characterise the material behaviour, and therefore serve to determine the critical temperature of the studied materials, is presented hereafter.

4.1. Assessment of the pyrolysis temperature

Table 4 shows the values of critical heat flux (CHF) below which the different insulation materials do not proceed to ignite with the horizontal set-up in the Cone Calorimeter (within 10 min). The three types of PIR show different values of critical heat flux, with PIRa being the most prone to ignite with a CHF of 10 kW·m^{-2}, while PIRb and PIRc show higher CHF of 12 and 15 kW·m^{-2} respectively. Phenolic foam shows the highest CHF for the plastic foams, with a CHF of 22 kW·m^{-2}. Stone wool did not ignite at any tested heat flux, which indicates that the failure criterion based on a critical temperature is not applicable, since the mix from the sparse generated pyrolysates could never reach the lean flammability limit.

Expanded polystyrene requires a special consideration. Since EPS tends to shrink rapidly once exposed to radiation from the Cone, actual values of CHF do not strictly correspond to the nominal flux at which the samples are initially exposed. No ignition was achieved before complete shrinkage of the sample for any of the studied cases. Critical heat flux values of 16 and 15 kW·m^{-2} were obtained assuming the external heat flux does not reduce at lower positions. Measurements of heat flux at lower positions, closer to the bottom of the sample, indicate that these tend to reduce approximately 35 % and 64 % for positions 50 mm and 100 mm lower, respectively. However, corrected heat fluxes would lead to inconsistent values of ignition temperature if the followed methodology is the one indicated in the previous section. Indeed, the ignition theory is defined on the basis of the semi-infinite solid assumption, and the use of the ignition theory for a thermally thin element would require to evaluate the shrinking time and pre-heating once the EPS film is formed.

Table 4. Critical heat flux obtained in the Cone Calorimeter

Critical heat flux / kW·m^{-2}					
PIRa	**PIRb**	**PIRc**	**PF**	**EPS**	**SW**
~ 10	~ 12	~ 15	~ 22	100 mm thick: ~ 16[2] equivalent to ~ 6 50 mm thick: ~ 15 equivalent to ~ 9 – 10	N/A

Pyrolysis temperatures are calculated considering a hypothetical absorptivity and emissivity of $\alpha = \varepsilon = 0.9$ and the global coefficient of heat losses as a function of the temperature (Eq. (5)). Calculated values for the different materials are presented in Table 5. The sensitivity of the ignition temperature calculation with regard to the uncertainty of the emissivity ($\pm$ 0.1) and the accuracy of the external heat flux measurement ($\pm$ 0.5 kW·m^{-2}) is indicated in Figure 3. Shaded regions are included in the plot, indicating variability with respect to the nominal value of assumed emissivity and heat flux. The error related to these uncertainties is low.

---

[2] This value refers to the heat flux at the surface before EPS starts shrinking. Actual heat flux at the bottom of the material where material accumulates is expected to be between 6 – 10 kW·m^{-2}

Table 5. Nominal values of calculated pyrolysis temperature

Pyrolysis temperature /°C					
PIRa	**PIRb**	**PIRc**	**PF**	**EPS**	**SW**
~ 306 ± 16	~ 337 ± 15	~ 377 ± 14	~ 453 ± 12	~ 305.9 – 389.4 (with CHF 10 – 16 kW·m^{-2})	N/A

However, the highest uncertainty lies on the quantification of the convective heat transfer coefficient. Unfortunately, this cannot be easily assessed, and the consistency of the obtained values of ignition temperature will be evaluated by comparison with data obtained from TGA for the determination of the critical temperature. In any case, values of global heat transfer coefficient, noted in Table 6, are consistent with the ones observed in the literature [26], with slightly larger values of convective coefficients herein. The uncertainty in the heat transfer coefficient is, however, tackled by considering an error region for the emissivity and heat flux, which compensates the likely overestimation of the convective coefficient.

Table 6. Estimated heat transfer coefficients

Convective, radiative and global heat transfer coefficient / W·m^{-2}·K^{-1}					
PIRa	**PIRb**	**PIRc**	**PF**	**EPS**	**SW**
$h_{conv} \approx 13.2$	$h_{conv} \approx 13.4$	$h_{conv} \approx 13.7$	$h_{conv} \approx 14.1$	$h_{conv} \approx 13.2 - 13.7$	N/A
$h_r \approx 19.1$	$h_r \approx 21.4$	$h_r \approx 24.9$	$h_r \approx 32.3$	$h_r \approx 19.1 - 26.0$	
$h_T \approx 32.3$	$h_T \approx 34.8$	$h_T \approx 38.5$	$h_T \approx 46.4$	$h_T \approx 32.3 - 39.7$	
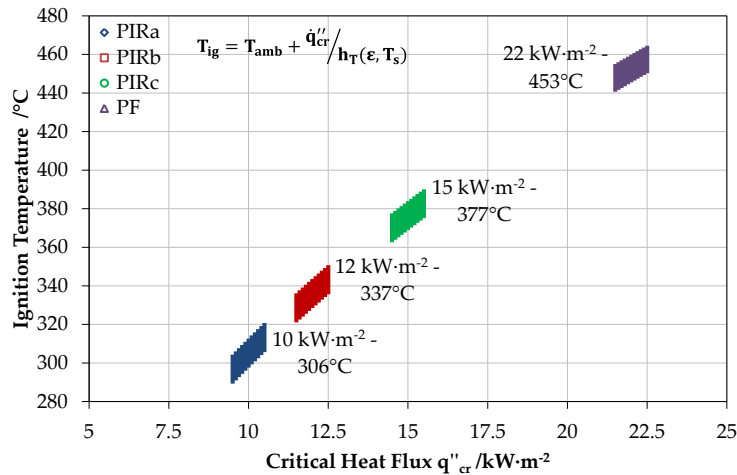
Figure 3. Calculated pyrolysis temperature for PIR and PF. Shading indicates sensitivity of the calculated variable to $\varepsilon \pm 0.1$ and $\dot{q}''_{cr} \pm 0.5 \text{ kW} \cdot \text{m}^{-2}$

4.2. Time-to-ignition and thermal inertia correlations

Scattered data of the inverse square root of time-to-ignition versus external heat flux for the three types of PIR and PF are presented in Figures 4 and 5. In general, results show good repeatability, although the inverse square root of time-to-ignition data at higher heat fluxes include larger scattering due to the very short ignition times that insulation materials experience under these conditions. Linear regressions representing the approach for the range $t_p/t_c \to 0$, noted in Equation (10), are included in

the charts from Figure 4a and 5a. Non-linear regressions representing the approach for the range $t_p/t_c \to \infty$, noted in Equation (11), are included in charts from Figure 4b and 5b.

Linear regressions ($t_p/t_c \to 0$) for PIR show a very poor agreement for any heat flux. However, the approach based on a non-linear regression ($t_p/t_c \to \infty$) seems to produce a better fitting, at least for the range up to 45 kW·m^{-2}. For the case of PF, the scatter data shows two clear trends: presented as a growing function from 22 to 40 kW·m^{-2} and as a horizontal function from 40 to 65 kW·m^{-2}, the latter representative of the relative importance of the transport/mixing period. The linear regression ($t_p/t_c \to 0$) for lower ranges of heat flux presents similar result to PIR, with a poor agreement. The fitting technique based on non-linear regression ($t_p/t_c \to \infty$) gives similar agreement, but replicates lower heat fluxes more accurately.
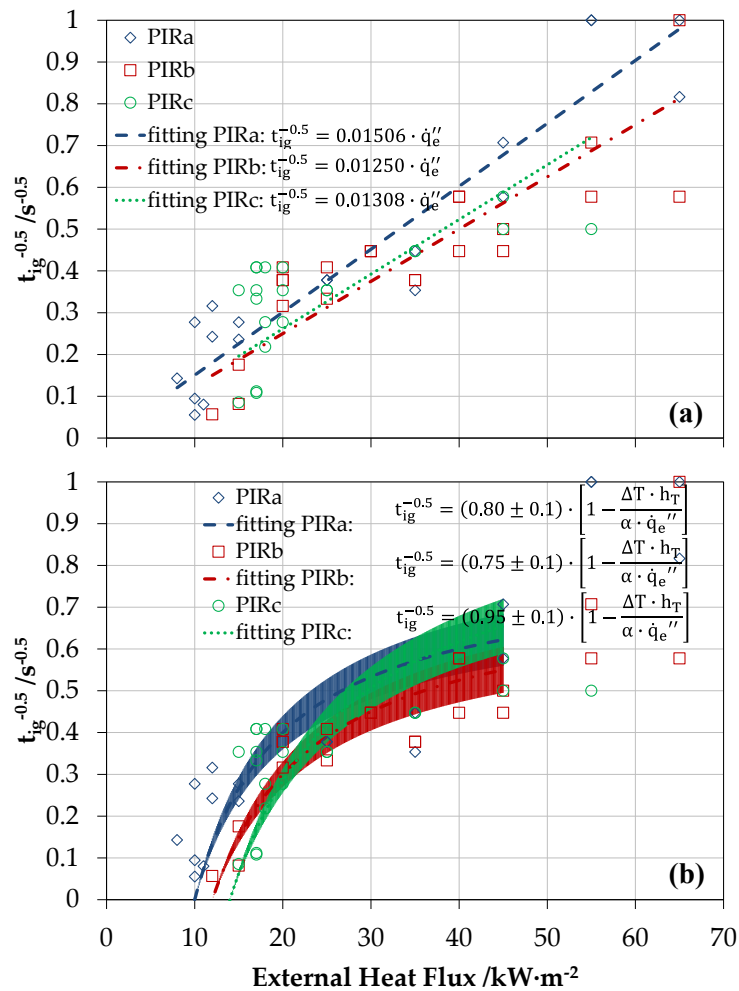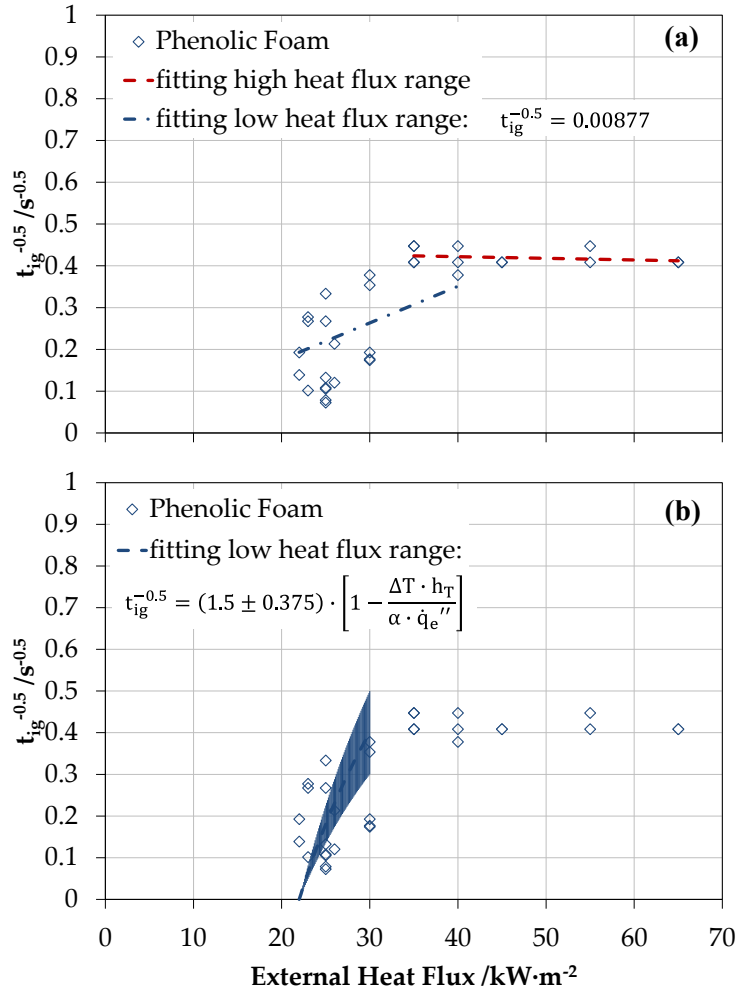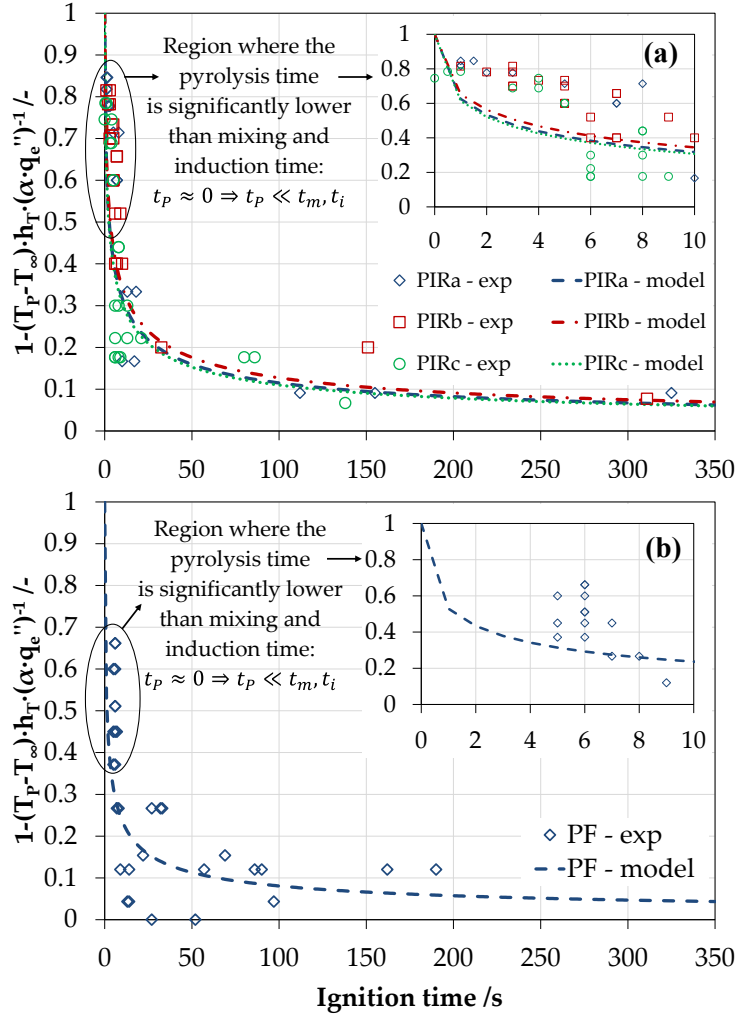

Figure 4. Time-to-ignition versus external heat flux of three PIR foams. Regressions based on Eq. (10) and Eq. (11)

Figure 5. Time-to-ignition versus external heat flux of PF. Regressions based on Eq. (10) and Eq. (11)

Figure 6 shows the obtained data processed by the function $f(t_p) = \left[1 - \frac{(T_P - T_\infty)}{T_c}\right]$ versus ignition times for PIR and PF. A relatively good fitting for ignition times longer than ten seconds is shown, while the fitting below ten seconds is relatively poor, with dissimilar trends between the fitting and the experimental data. This disagreement is indicative of pyrolysis times near zero seconds, thus the mixing and induction time playing an important role; consequently, correlations of thermal inertia near this region are expected to provide erroneous quantification.

Figure 6. Time-to-ignition versus external heat flux of (a) three PIR foams and (b) PF based on Eq. (12)

Calculated values of thermal inertia obtained by the three different approaches introduced above are presented in Table 7. It is shown that the approach established for the domain $t_p/t_c \to 0$ offers relatively large values of thermal inertia in comparison to the approach usually followed for the domain $t_p/t_c \to \infty$ and the approach proposed by the authors, which present good agreement and have a similar order of magnitude as the values of thermal inertia at ambient temperature. This confirms that the regression based on the domain $t_p/t_c \to 0$ is not suitable for materials with low thermal inertia. Values of thermal inertia for SW are not calculated since no ignition was achieved, while values of thermal inertia for EPS are not calculated since the material shrinks and melts, becoming a thermally thin element, therefore, the thermal inertia having no physical meaning for this case.

The calculated values of thermal inertia, as well as the small ignition times, indicate again the propensity of the insulation materials to ignite quickly and with low energy inputs. This reinforces the view that the proper design of thermal barriers is imperative to control the onset of pyrolysis.

17

Table 7. Nominal values for calculated thermal inertia

$k\rho c$ /W^2·s·K^{-2}·m^{-4}						
Range	**PIRa**	**PIRb**	**PIRc**	**PF**	**EPS**	**SW**
$t_p/t_c \to 0$ Eq. (10)	$\sim 55 \cdot 10^3$	$\sim 66 \cdot 10^3$	$\sim 47 \cdot 10^3$	$\sim 71 \cdot 10^6$	N/A	N/A
$t_p/t_c \to \infty$ Eq. (11)	$\sim 5.1 \cdot 10^3$	$\sim 6.1 \cdot 10^3$	$\sim 5.2 \cdot 10^3$	$\sim 3.0 \cdot 10^3$	N/A	N/A
$f(t_p) = \left[1 - \dfrac{(T_P - T_\infty)}{T_c} \right]$ Eq. (12)	$\sim 4.5 \cdot 10^3$	$\sim 6.5 \cdot 10^3$	$\sim 5.5 \cdot 10^3$	$\sim 4.5 \cdot 10^3$	N/A	N/A

4.3. Thermal degradation at material scale

The mass loss experienced by temperature increases for the different insulation materials during the TGA experiments is presented below. These results are expressed as a normalised variable, being the ratio between the measured value and the initial sample mass.

Figure 7a presents the normalised mass of SW in a nitrogen atmosphere. The total mass loss for most of the heating rates is lower than 1 % at the reference temperature of 800 °C. Only one experiment, run with a heating rate of 2.5 °C·s^{-1}, presents a greater mass loss, totalling approximately 2 % at 800 °C, probably because the sample was prepared from a region of the insulation with higher binder content, or due to an erroneous blank subtraction technique. All mass loss curves show a main drop of mass between 200 °C and 350 °C, which is representative of the pyrolysis of the binder or additives. Figure 7b presents the normalised mass in an air atmosphere. The total mass loss for all the heating rates is between 1 % and 1.5 % at the reference temperature of 400 °C. Two steps of mass loss are observed between 200 °C and 450 °C, representing the pyrolysis reaction observed in nitrogen and an additional oxidation reaction. A plateau in mass is observed between 450 °C and 700 °C, with a slight increase of mass from 700 °C, which is representative of a crystallisation reaction.
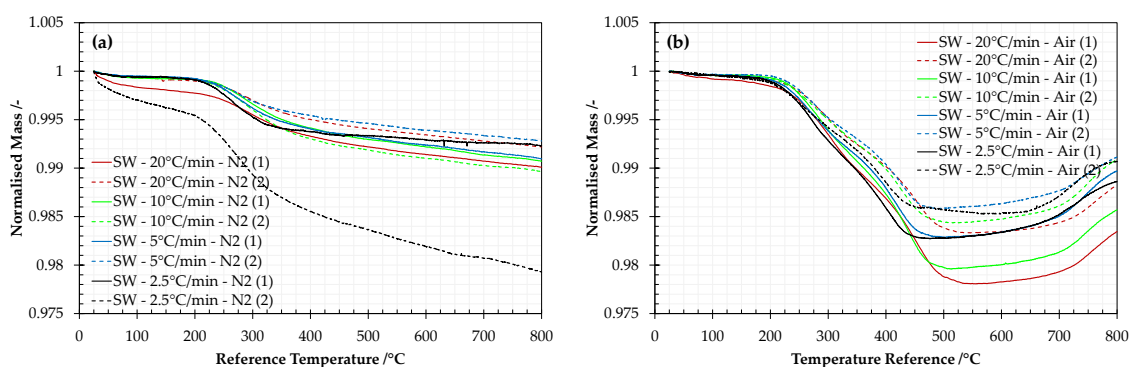
Figure 7. Thermal degradation of SW under different heating rates in nitrogen (a) and air (b) atmospheres at 50 ml·min^{-1}

Mass loss results due to thermal degradation processes in a nitrogen atmosphere for four different heating rates and the three different PIR foams are presented in Figure 8. PIRa, PIRb and PIRc show a total mass loss of approximately 76 % at a reference temperature of 800 °C. The residues after the experiments present a typical char structure, black and porous. It is identified that the main mass loss

step for the three PIR foams is produced between 250 °C and 450 °C, which is representative of the main pyrolysis process. Lower heating rates present higher mass loss than higher heating rates for the same reference temperature, with good repeatability between tests with the same heating rate.
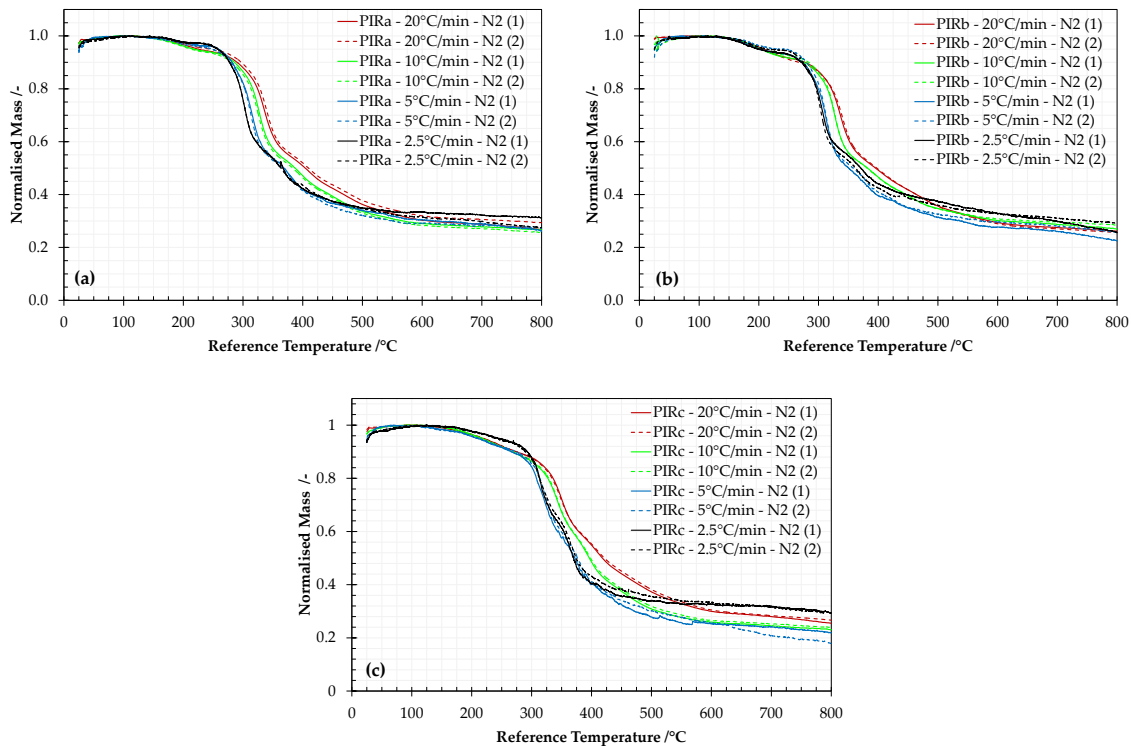

Figure 8. Thermal degradation of (a) PIRa, (b) PIRb and (c) PIRc under different heating rates in a nitrogen atmosphere (50 ml·min⁻¹)

Mass loss due to thermal degradation processes in an air atmosphere for four different heating rates and the three different PIR foams is presented in Figure 9. The mass loss curves for the three types of foam mainly consist of two steps. Similarly to the experiments in nitrogen, the first steep drop of mass is presented between 250 °C and 350 °C approximately, following a gentle drop of mass after 150 °C, while the second steep drop of mass is presented between 350 °C and 600 – 700 °C, which is representative of char oxidation. In general, a pattern of curves from lower heating rates being displaced to lower temperatures is observed. PIRa and PIRb show similar behaviour up to 350°C, presenting the steepest mass loss steps and achieving an approximate average of remaining mass of 64 % and 59 %, respectively, at this temperature. On the contrary, PIRc presents a gentler mass loss drop up to 350 °C, achieving an average remaining mass of 72 %.
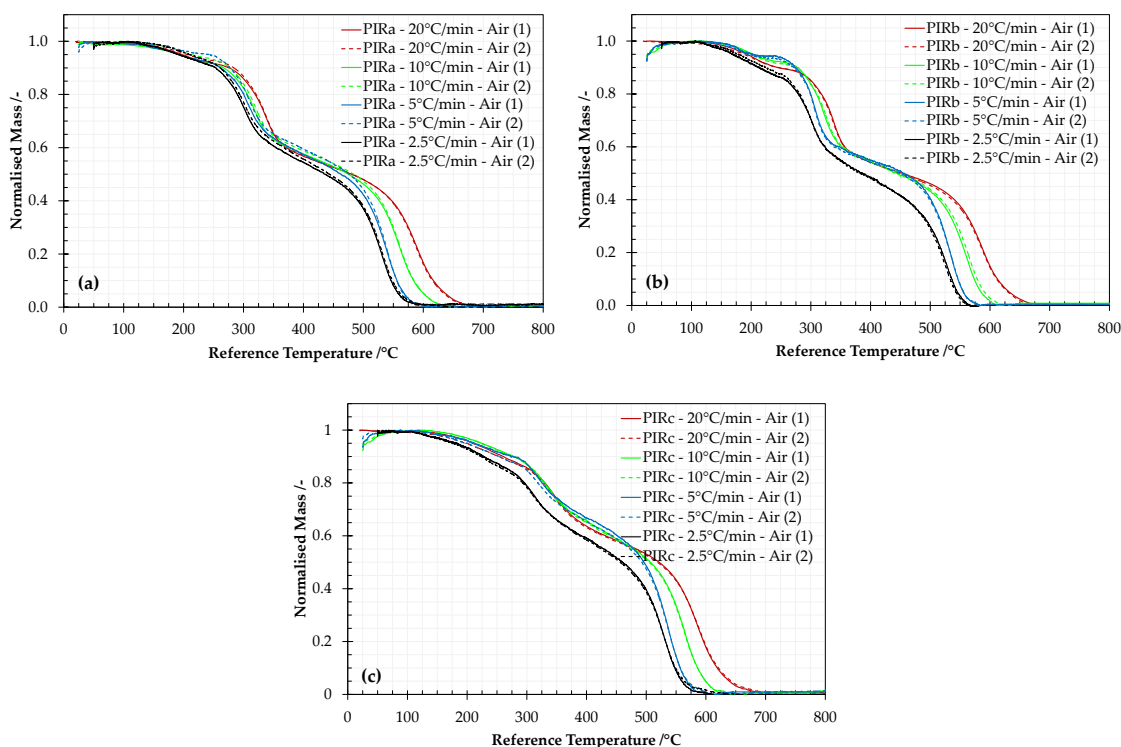
Figure 9. Thermal degradation of (a) PIRa, (b) PIRb and (c) PIRc under different heating rates in an air atmosphere (50 ml·min^{-1})

Figure 10a presents the mass loss of PF in a nitrogen atmosphere. Two main steps of mass loss can be identified: the first approximately between 200 °C and 350 °C, and the second and steepest step between 350 °C and 500 °C, followed by a plateau with low mass loss up to 800 °C. The total mass loss at a reference temperature of 800 °C is approximately 63 %. Figure 10b shows the mass loss of PF in an air atmosphere, with two main steps of mass loss being identified: the first between 200 °C and 300 °C, followed by very sharp mass loss from 400 °C up to 500 – 600 °C. The mass is completely consumed after 600 °C. In general, good agreement is found between different heating rates. Slower heating rates show steeper mass loss in the second step, although this is not clearly observed for the first step of mass loss.
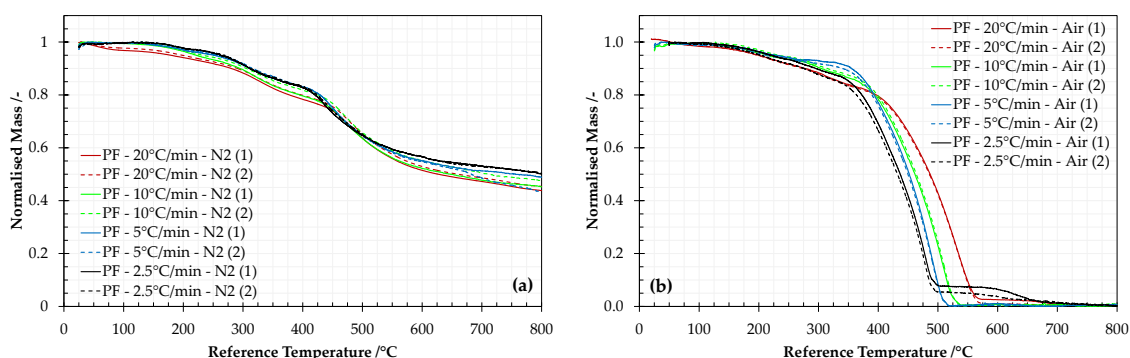
Figure 10. Thermal degradation of PF under different heating rates in nitrogen (a) and air (b) atmospheres at 50 ml·min^{-1}

Figure 11a shows the mass of EPS samples in a nitrogen atmosphere. A single main drop in the mass is observed between 350 °C and 450 – 475 °C, with all mass being consumed at the latter reference temperature; therefore, no significant residue is found after the tests were ended at 800 °C. Good repeatability is found between the different tests run at the same heating rate. Figure 11b presents the loss of mass in an air atmosphere. Apparently a single mass loss drop is observed for all heating rates from 300 °C to 425 °C, but with non-uniform slope between them. All mass is consumed after this single mass drop, with no apparent residue observed after 800 °C. The repeatability of the tests is found to be poor in comparison with the tests run in nitrogen. This is attributed to the diffusion of oxygen through the surface of the sample, affecting the pyrolysis behaviour, and being dependent on the size or morphology of the sample.
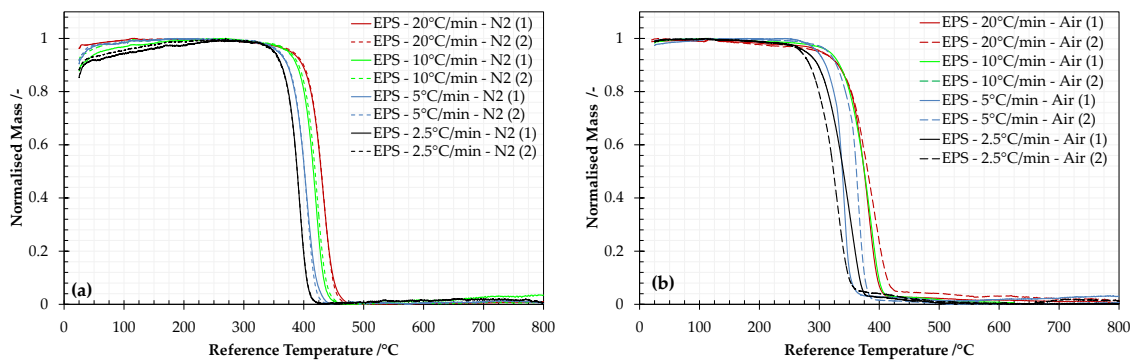
Figure 11. Thermal degradation of EPS under different heating rates in nitrogen (a) and air (b) atmospheres at 50 ml·min⁻¹

5. Discussion

As noted by *Hidalgo et al.* (2015a), the performance-based methodology requires the definition of a critical temperature for each particular insulation material, which represents the onset of fire hazard (heat release contribution, generation of toxic species and breaching of compartmentalisation) [12]. The use of this parameter with the thermal properties and thickness of the thermal barrier, and a series of fire scenarios jointly set the optimisation problem for the design of building assemblies which aims at delivering assemblies with an equivalent level of safety, independent of the insulation material used [14]. The selection of results presented in the previous section provide the baseline to establish values of critical temperature for each of the insulation materials studied.

The pyrolysates from plastic foams PIR, PF and EPS have been demonstrated to be flammable and the materials themselves have been shown to degrade (thermally and mechanically) after the onset of pyrolysis, therefore a failure criterion based on a critical pyrolysis temperature can be considered valid for representing the hazard of significant release of pyrolysis gases. The use of this approach towards establishing a failure criterion for stone wool insulation with low binder content is not so clear. First, for this material a flammable mixture cannot be obtained, thus it is not possible to establish a critical

heat flux for ignition. This is supported by the TGA results which indicate a maximum percentage of mass loss up to 2 % of the total mass for stone wool, which will not sustain a flame.

Whereas it is commonly known that inorganic insulation does not normally ignite and produces low emissions [30], a larger content of binder could potentially represent a fire hazard. Therefore, it is advised that the assessment method presented in this work is also pursued for any other type of inorganic material with different content of binder, to additionally verify that the amount of products generated by the binder pyrolysis and oxidation do not represent a hazard.

Flammability experiments provide a series of pyrolysis temperatures for rigid plastic that are indicative of the likely critical temperature representative of the onset of pyrolysis. The obtained pyrolysis temperatures represent an estimation of the *flash point*, i.e. the point at which the mass flux of pyrolysis gases provides sufficient fuel for the a flammable mixture to be attained and thus allow piloted ignition [34]. This methodology was however shown not to be suitable for determining the ignition temperature for EPS due to its shrinking behaviour.

An alternative approach is to establish the temperature at which maximum gasification occurs. This temperature will be unavoidably different to that established from the critical heat flux for ignition, nevertheless in this study it will be assumed that the difference between both is not significant. Then, an assessment of the temperature of maximum gasification is necessary, which can be achieved by evaluating the differential form of the thermo-gravimetric results presented above.

A selection of the obtained rates of mass loss from thermo-gravimetric analyses under nitrogen and air atmospheres at the slowest heating rate used are presented in Figure 12. Since DTG curves implicitly carry a low signal-to-noise ratio, these curves have been smoothened by using locally weighted scatterplot smoothing (LOESS) [35]. The calculated value of pyrolysis temperature and uncertainty in the calculation are presented in the figure as vertical dashed lines and shadings, respectively. A good agreement is found between the calculated pyrolysis temperature and those at which the main peaks of mass loss rate are obtained by thermogravimetry, with the pyrolysis temperature shifted to higher values of temperature. This provides the necessary validation for the assumption that maximum gasification temperatures are very similar to the pyrolysis temperatures estimated from the piloted ignition tests.

It should be noted that since these foams are closed-cell polymers, the solid oxidation is only expected at the surface after the material has pyrolysed. Additionally, the air is hindered at the surface of the insulation by the thermal barrier, unless the material shrinks or melts, such as with EPS. Thus, the thermo-gravimetric results addressed for PIR and PF should refer to purely nitrogen atmospheres, with absence of oxygen, while results addressed for EPS should refer to air conditions.

Despite the fact that the peak temperature in DTG does not directly indicate a property of the specific decomposition reaction, since it tends to shift to higher temperatures at higher heating rates, it

can be used to define the critical temperature. Indeed, if a sufficiently low heating rate is chosen, the peak temperature in DTG then provides a conservative value of temperature with the highest rate of mass loss. Therefore, the proposed values of critical temperature considering this approach are presented in Table 8. The three different PIR foams have shown different pyrolysis behaviour, with PIRc showing a larger pyrolysis temperature. However, a conservative generic value of the critical temperature may be indicated by 300 °C, while the proposed conservative critical temperature for PF is 425 °C.

Expanded polystyrene, however, requires a special consideration due to its melting behaviour. Although a value of 330 °C has been identified as the main peak of DTG in Figure 12, the authors believe that consideration should also be given to the melting temperature. Indeed, while the hazard from rigid foams such as PIR and PF may be represented by the direct pyrolysis without experiencing melting (solid→gas), the hazard from EPS must also be represented by the melt prior to pyrolysis (solid→melt→gas), which could transport to the compartment. Therefore, a conservative critical temperature for EPS can be represented by its melting point. Unfortunately values of melting point could not be obtained directly by the current experimental programme; thus, a value of 240 °C given by *Wunsch* [36] is adopted. This consideration is included as an additional criterion for onset of hazard to further illustrate the limits of the present methodology. The natural complexity of these materials requires all these considerations if quantitative performance criteria are to be established for designers.

Table 8. Proposed values of critical temperature

T_{cr} /°C					
PIRa	**PIRb**	**PIRc**	**PF**	**EPS**	**SW**
~ 300	~ 300	~ 360	~ 425	~ 240	N/A
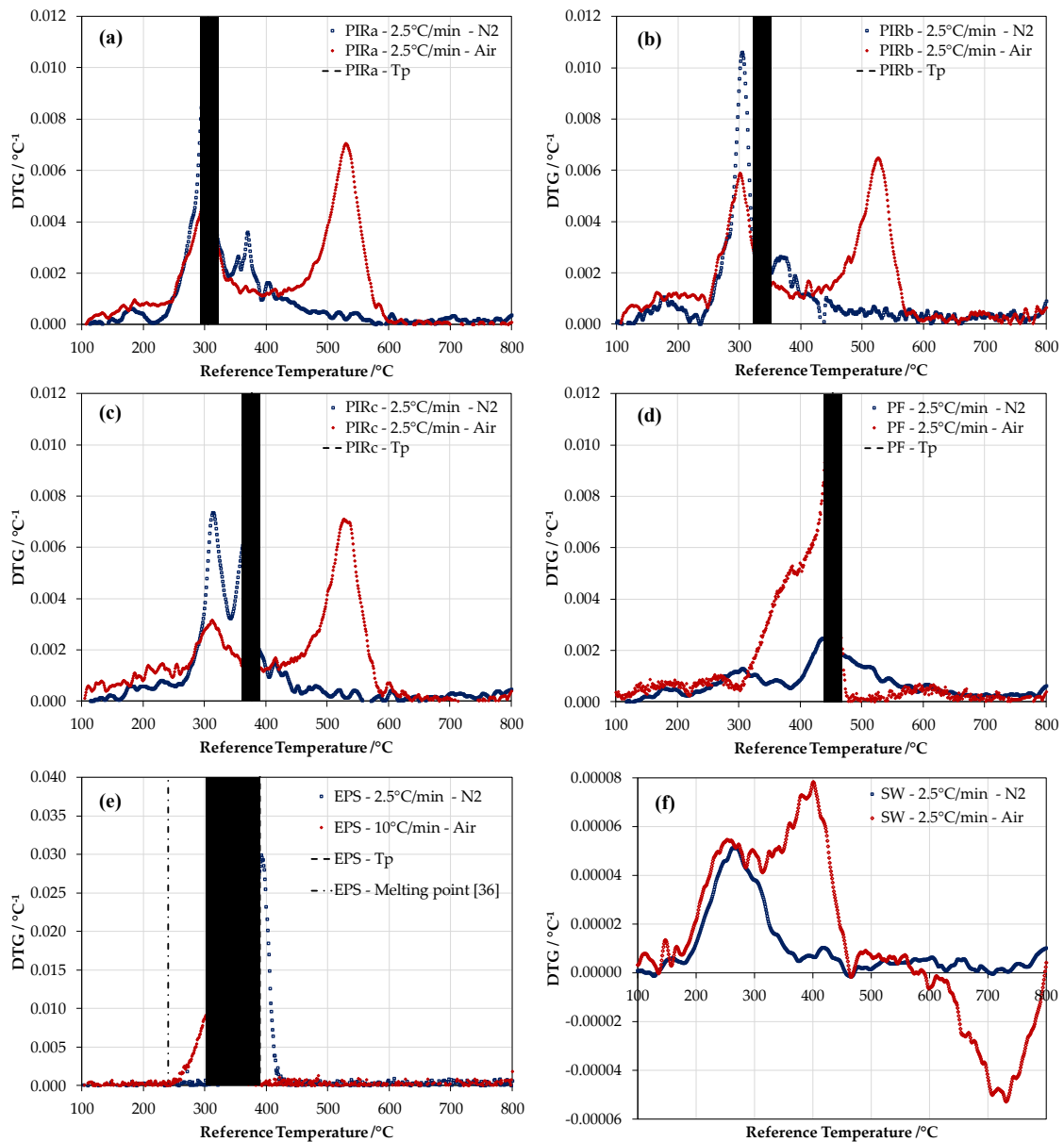
Figure 12. Differential thermo-gravimetric curves of (a) PIRa, (b) PIRb, (c) PIRc, (d) PF, (e) EPS and (f) SW at nitrogen and air atmosphere at 50 ml·min^{-1}. Shading indicates the range of uncertainty from the calculated ignition temperature

6. Conclusions

The concept of critical temperature has been proposed so as to represent the onset of hazard for insulation materials. Coincidence has been found when considering the pyrolysis temperature extracted from piloted ignition studies (Cone Calorimeter) and when considering the temperature at which the material experiences maximum gasification. While this approach does not fully reflect the process of pyrolysis, it provides a conservative and simple condition that can actually be measured, thus allowing a quantitative design to be performed by using a simplified heat transfer methodology.

An assessment of the critical temperature for a series of insulation materials has been provided and the approach showed to be valid for insulation that does not experience shrinkage. It was observed that

the temperature of the main peak of pyrolysis obtained from differential thermal analysis (DTG) under a nitrogen atmosphere at low heating rates is lower than the piloted ignition temperature in the Cone Calorimeter. Thus, to remain conservative, the conditions recommended for the critical temperature selection are a heating rate of 2.5 °C·min^{-1} and atmospheric conditions in absence of oxygen. However, for materials that shrink and melt, it is suggested to consider the melting point as a potentially more conservative definition of the critical temperature. Arguably this could be replaced by the temperature of the main peak of pyrolysis obtained from DTG under oxidative conditions, if it is demonstrated that the transport from the EPS melt to the compartment or the changes of mechanical integrity of the system do not result in a hazard. Therefore, conservative values of critical temperature proposed are 300 °C for polyisocyanurate, 425 °C for phenolic foam and 240 °C for expanded polystyrene (to the nearest 5 °C). The present approach does not apply for the particular low density stone wool studied here because the release of flammable volatiles from the material are insufficient to achieve a flammable mixture.

Stone wool, polyisocyanurate foam, phenolic foam and expanded polystyrene are the main focus of this work, but further research would be required in order to identify the critical temperature of other common insulators, e.g. inorganic insulation based on glass fibre, organic materials such as polyurethane, cork, sheep-wool and cellulose-based insulation, or combined and new technology materials.

Acknowledgements

References

1. (2009) BS EN 13501-1. Fire classification of construction products and building elements. Part 1: Classification using data from reaction to fire tests.

2. (2012) BS EN 1363-1. Fire resistance tests — Part 1: General Requirements.

3. (2010) BS EN ISO 1182. Reaction to fire tests for products — Non-combustibility test.

4. (2010) BS EN ISO 1716. Reaction to fire tests for products — Determination of the gross heat of combustion (calorific value).

5. (2010) BS EN ISO 11925-2. Reaction to fire tests — Ignitability of products subjected to direct impingement of flame. Part 2: Single-flame source test.

6. (2010) BS EN ISO 13823. Reaction to fire tests for building products — Building products excluding floorings exposed to the thermal attack by a single burning item.

7. (2014) 2015 International Building Code - IBC. International Code Council, Inc., USA

8. (2015) NFPA 5000 - Building Construction and Safety Code.

9. (2014) ASTM E84. Standard Test Method for Surface Burning Characteristics of Building Materials.

10. (2012) ASTM E119. Test Methods for Fire Tests of Building Construction and Materials. doi: 10.1520/e0119-12a

11. (1993) ISO 9705. Fire tests — Full-scale room test for surface products.

12.   Hidalgo JP, Welch S, Torero JL (2015) Performance criteria for the fire safe use of thermal insulation in buildings. Constr Build Mater 100:285–297. doi: 10.1016/j.conbuildmat.2015.10.014

13.   Drysdale DD (1986) Fundamentals of the Fire Behaviour of Cellular Polymers. In: Fire Cell. Polym. Springer Netherlands, Dordrecht, pp 61–75

14.   Hidalgo JP, Welch S, Torero JL (2015) Design Tool for the Definition of Thermal Barriers for Combustible Insulation Materials. Proc. 2nd IAFSS Eur. Symp. Fire Saf. Sci.

15.   Lautenberger C, Fernandez-Pello C (2009) Generalized pyrolysis model for combustible solids. Fire Saf J 44:819–839. doi: 10.1016/j.firesaf.2009.03.011

16.   Wasan SR, Rauwoens P, Vierendeels J, Merci B (2010) An enthalpy-based pyrolysis model for charring and non-charring materials in case of fire. Combust Flame 157:715–734. doi: 10.1016/j.combustflame.2009.12.007

17.   Drysdale D (2011) An Introduction to Fire Dynamics, 3rd ed. Wiley

18.   (1993) BS 476-15, ISO 5660-1. Fire tests on building materials and structures. Method for measuring the rate of heat release of products.

19.   Beyler CL, Hirschler MM (2002) Thermal Decomposition of Polymers. In: DiNenno PJ, Drysdale D, Beyler CL, et al (eds) SFPE Handb. Fire Prot. Eng., 3rd ed. National Fire Protection Association, Massachusetts, U.S.A., pp 1–110 to 1–131

20.   Quinn S (2001) Chemical blowing agents: providing production, economic and physical improvements to a wide range of polymers. Plast Addit Compd 3:16–21. doi: 10.1016/S1464-391X(01)80162-8

21.   Dominguez-Rosado E, Liggat JJ, Snape CE, et al (2002) Thermal degradation of urethane modified polyisocyanurate foams based on aliphatic and aromatic polyester polyol. Polym Degrad Stab 78:1–5. doi: 10.1016/S0141-3910(02)00086-1

22.   Babrauskas V, Twilley WH, Parker WJ (1993) The effects of specimen edge conditions on heat release rate. Fire Mater 17:51–63. doi: 10.1002/fam.810170202

23.   (2009) ASTM E 2058. Standard Test Methods for Measurement of Synthetic Polymer Material Flammability Using a Fire Propagation Apparatus (FPA). doi: 10.1520/E2058-09

24.   Maani AQ (2013) Effects of Oxygen Concentration on the Smouldering Combustion of the Rigid PIR Insulation Material (M.Sc. thesis). The University of Edinburgh

25.   Rasbash DJ (1976) Theory in the evaluation of fire properties of combustible materials. Proc 5th Int Fire Prot Semin (Karlsruhe, Sept 113–130.

26.   Janssens M, Kimble J, Murphy D (2003) Computer tools to determine material properties for fire growth modeling from cone calorimeter data. In: Fire Mater. 8th Int. Conf. Int. Conf. San Francisco, CA, pp 377–387

27.   Long RT, Torero JL, Quintiere JG, Fernandez-Pello AC (1999) Scale and transport considerations on piloted ignition of PMMA. In: Sixth Int. Symp. Fire Saf. Sci. pp 567–578

28.   Lloyd JR, Moran WR (1974) Natural Convection Adjacent to Horizontal Surface of Various Planforms. J Heat Transfer 96:443. doi: 10.1115/1.3450224

29.   Mowrer F (2005) An analysis of effective thermal properties of thermally thick materials. Fire Saf J 40:395–410. doi: 10.1016/j.firesaf.2005.03.001

30.   Hidalgo-Medina JP (2015) Performance-based methodology for the fire safe design of insulation materials in energy efficient buildings (Ph.D. thesis). The University of Edinburgh

31.   Gabbot P (2008) Principles and Applications of Thermal Analysis. Blackwell Publishing Ltd.

32. Sánchez-Jiménez PE, Pérez-Maqueda L a, Perejón A, Criado JM (2013) Clarifications regarding the use of model-fitting methods of kinetic analysis for determining the activation energy from a single non-isothermal curve. Chem Cent J 7:25. doi: 10.1186/1752-153X-7-25

33. Pérez-Maqueda LA, Criado JM, Sanchez-Jiménez PE (2006) Combined kinetic analysis of solid-state reactions: a powerful tool for the simultaneous determination of kinetic parameters and the kinetic model without previous assumptions on the reaction mechanism. J Phys Chem A 110:12456–62. doi: 10.1021/jp064792g

34. Torero JL (2008) Flaming ignition of solid fuels. SFPE Handb. Fire Prot. Eng.

35. Cleveland WS, Devlin SJ (1988) Locally Weighted Regression: An Approach to Regression Analysis by Local Fitting. J Am Stat Assoc 83:596–610. doi: 10.1080/01621459.1988.10478639

36. Wünsch JR (2000) Polystyrene – Synthesis, Production and Applications. iSmithers Rapra Publishing